Mem. S.A.It. Vol. 81, 654

Memorie della

Solar quiescent prominences

Filamentary structure and energetics

P. Heinzel[1], U. Anzer[2], and S. Gunár[1]

[1] Astronomical Institute, Academy of Sciences, 25165 Ondřejov, Czech Republic
e-mail: pheinzel@asu.cas.cz
[2] Max-Planck-Institut für Astrophysik, Karl-Schwarzschild-Strasse 1, 85740 Garching, Germany

Abstract. We present a first attempt to solve the non-LTE radiative-transfer problem within a 2D numerical domain consisting of several randomly distributed vertical threads. This represents a starting point to simulate mutual radiative interaction between such prominence threads. The second part of the paper presents our new results which concern the radiative equilibrium in prominences and in their fine structure. We show that adding the non-hydrogenic radiative losses significantly lowers the central equilibrium temperatures. To match the observed temperatures, an additional heating seems to be unavoidable.

Key words. Line: formation – Line: profiles – radiative transfer – Sun: chromosphere – Sun: prominences

1. Introduction

Most solar quiescent prominences show bundles of quasi-vertically aligned narrow threads (Heinzel et al. 2008, and Fig. 1) which exhibit some small-scale dynamics as demonstrated by Berger et al. (2008) or Schmieder et al. (2010). On the other hand, the prominence magnetic field seems to be predominantly horizontal and thus the question arises how the vertical plasma thread can be suspended in an almost horizontal field. There are basically two complementary scenarios which apply to weak (say below 10 Gauss) and stronger (tens of Gauss) fields, respectively. Provided that the gas pressure derived from spectral diagnostics is in the range 0.1–1 dyn cm^{-2}, these two limits correspond to plasma β up to one or much lower than one, respectively. If β is non-negligible, the gravity-induced magnetic dips filled with the plasma will form a vertically aligned thread as described below. On the other hand, pre-dipped force-free fields may also form similar threads as recently shown by Dudík et al. (2008). In both cases, a non-LTE transfer modeling for such a thread geometry has to be used in order to explain the observed radiation properties of quiescent prominences.

Send offprint requests to: P. Heinzel

1.1. MHS equilibrium

The magneto-hydrostatic (MHS) pressure balance originally derived by Kippenhahn & Schlüter (1957) can be ex-

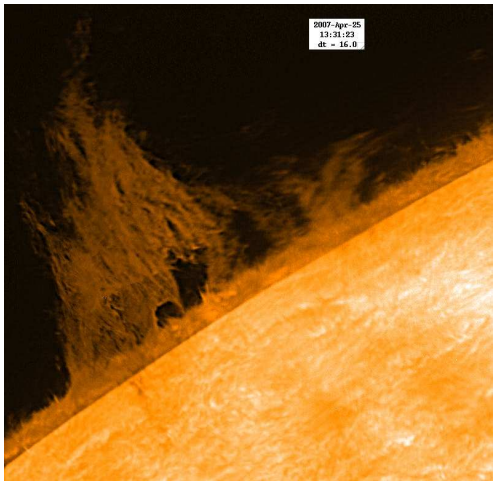

Fig. 1. Quiescent prominence observed in the Hα line by the *Hinode* satellite (SOT). Note the quasi-vertical fine-structure plasma threads. From Heinzel et al. (2008).

pressed using the column-mass coordinate m, having

$$\mathrm{d}m = -\rho \mathrm{d}x\,, \tag{1}$$

where ρ is the the plasma density and x the geometrical coordinate. $m = 0$ at one surface of the prominence slab or thread and $m = M$ at the opposite one. Loading of such a mass into an initially horizontal magnetic field leads to the formation of a gravity-induced dip. The pressure-balance equation for such a 1D dip configuration reads

$$p(m) = 4p_\mathrm{c}\frac{m}{M}\left(1-\frac{m}{M}\right)+p_0\,, \tag{2}$$

where p is the gas and turbulent pressure and p_0 is the coronal pressure at the surfaces. This equation was first derived by Heasley & Mihalas (1976) and used to model prominences as a whole. At the surface one has the vertical component of the field vector $B_z \equiv B_{z1}$ which gives, together with the horizontal component $B_x = \mathrm{const.}$, the total mass loading M

$$M = \frac{B_x B_{z1}}{2\pi g}\,. \tag{3}$$

Using this relation, we obtain for p_c

$$p_\mathrm{c} = \frac{B_{z1}^2}{8\pi}\,. \tag{4}$$

p_c has the meaning that at the center we have the pressure

$$p_\mathrm{cen} = p(M/2) = p_\mathrm{c} + p_0\,. \tag{5}$$

If p_0 would be zero, then $p_\mathrm{cen} = p_\mathrm{c} = B_{z1}^2/8\pi$ and the pressure at the center will be equal to the magnetic pressure calculated with $B = B_{z1}$. This formulation with the column mass has a great advantage of being valid for any temperature and ionization-degree distribution. To get the density ρ we use the state equation with the mean molecular mass

$$\mu = \frac{1+4\alpha}{1+\alpha+i}m_\mathrm{H}\,, \tag{6}$$

where i is the ionization degree of hydrogen $i = n_\mathrm{p}/n_\mathrm{H}$ (n_p and n_H are the proton and hydrogen densities, respectively), α the helium abundance relative to hydrogen and m_H the hydrogen atom mass. i varies between zero (neutral gas) and unity (fully-ionized plasma). Inside the prominence and the prominence-corona transition region (PCTR), one can consider some schematic variation of i with depth but for a specific prominence model the true ionization-degree structure results from rather complex non-LTE radiative-transfer calculations. Therefore, the evaluation of the MHS equilibrium must be coupled to the non-LTE transfer. This 1D MHS equilibrium was then generalized to two-dimensional (2D) case, which represents the basis of 2D models of the fine-structure vertical threads (Heinzel & Anzer 2001).

1.2. 2D multi-thread radiative transfer

2D multi-thread models consist of a set of identical single 2D threads placed into a larger mesh and irradiated from all sides from the solar surface. Individual threads are precomputed using a 2D thread model (Heinzel & Anzer 2001) which considers vertically infinite 2D fine-structure threads embedded in dips of the horizontal magnetic field. The variation of all

physical quantities occurs in a horizontal plane parallel to the solar surface. The 2D MHS-equilibrium of these fine-structure models was discussed by Heinzel & Anzer (2001), where an empirical temperature profile was assumed. The temperature structure is characterized by two different shapes of the PCTR. Within a narrow PCTR layer across the magnetic field lines the temperature exhibits a steep gradient between the central coolest part of the thread and its boundaries. In contrast, the temperature increases gradually along the field lines within a rather extended PCTR layer.

For solving the 2D radiative transfer in a heterogeneous medium represented by 2D vertical threads placed into otherwise empty space we have modified the 2D solver used by Heinzel & Anzer (2001). This is based on the Accelerated Lambda Iteration (ALI) technique developed by Auer & Paletou (1994) with the usage of the Short Characteristics (SC) method for obtaining the formal solution along individual rays. We assume a 5-level hydrogen plus continuum atom and use partial redistribution for the Lα and Lβ lines (Paletou 1995). The non-LTE statistical equilibrium equations are preconditioned according to Rybicki & Hummer (1991) (MALI) and then linearized with respect to the particle number densities to compute the hydrogen ionization balance (Heinzel 1995). The number of rays per octant was chosen to be 12 and we used the the same abscissae and weights as in (Heinzel & Anzer 2001).

To study the mutual radiative interaction of threads we first compute a fully consistent model of a single 2D thread. Then we randomly place a number of identical 2D threads with precomputed temperature, density, electron density, and magnetic field variations into a large computational domain. Next we apply the incident solar radiation at the domain boundaries and again solve the non-LTE problem. This results in new source-function distributions for each thread within the computational domain. Finally, we formally integrate the transfer equation along a given line of sight.

1.3. Effects of mutual radiative interaction

The comparison of the Lyman line profiles obtained with multi-thread models with and without mutual radiative interaction shows that the profiles obtained with the mutual radiative interaction exhibit a significant increase of the intensity in the peaks, compared to models without interaction (Fig. 2, bottom). This effect is due to mutual irradiation of the central parts of individual threads, where the intensity in the line peaks is much higher than the incident radiation from the solar surface (up to a factor of three). The behavior of the mutual radiative interaction can be better seen from its effect on the source function, e.g., at the center of the Lα line (Fig. 2, top). The problem is that taking into account the mutual radiative interaction in the way described here, the peak-to-center ratio for Lα and Lβ lines increases, contrary to what is observed (Gunár et al. 2010). Therefore, further development of this complex modeling is required.

2. Prominence energetics

The energetics is rather different in the central cool parts of the prominence structures and in the PCTR. In the former case, at temperatures below say 2×10^4 K, optically-thick transitions require the full non-LTE radiative-transfer modeling in order to determine the radiative losses. This was done for hydrogen by Heasley & Mihalas (1976), Anzer & Heinzel (1999) or recently by Gouttebroze (2007). Heinzel & Anzer (2010) added other losses as discussed below. Inside the PCTR, at higher temperatures, optically-thin losses are usually considered (e.g., Parenti & Vial 2007; Anzer & Heinzel 2008). Thin losses are also used in RHD simulations where the temperatures are limited down to 3×10^4 K. A more comprehensive modeling was done by Fontenla et al. (1996) and Anzer & Heinzel (1999) who solved the transfer problem for hydrogen and added optically-thin losses for other elements. However, this approach is somewhat tricky and rather uncertain for the cool central parts. Possible heating mecha-

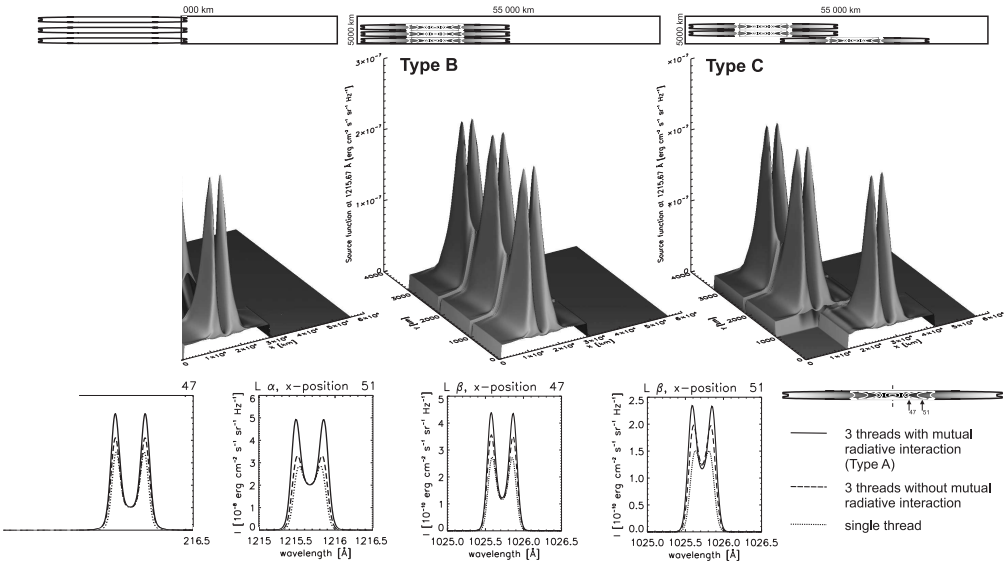

Fig. 2. Top: Variation of the source function at the Lα center. The x and y axes show the geometrical dimensions of the computational mesh. Note that these plots are not drawn to the proper scale. The proper geometrical scale is indicated by schematic sketches which also show the placement of the threads. Bottom: Emerging Lα and Lβ profiles for three different scenarios and at two positions indicated in the sketch on the right.

nisms which can be considered under prominence conditions are:

- radiation (in lines and continua)
- heat conduction
- ambipolar diffusion
- transport of ionization energy
- magnetic heating (reconnection, waves)
- mechanical heating (shocks, flow dissipation)
- enthalpy heating.

2.1. Energy balance

In case of radiative equilibrium, the radiative flux integrated over all frequencies is conserved inside the prominence slab. This also means that the total radiative energy emitted at a given point must be exactly equal to that absorbed, i.e., the net radiative losses

$$L = 4\pi \int_0^\infty (\eta_\nu - \chi_\nu J_\nu) \mathrm{d}\nu \qquad (7)$$

must be equal to zero (here η and χ are the emission and absorption coefficients, respectively, and J the mean radiation intensity). But generally there exist sources of heating and cooling which establish the energy equilibrium. The energy balance equation then reads

$$\frac{\mathrm{d}F_\mathrm{c}}{\mathrm{d}x} = L - H\,, \qquad (8)$$

where l.h.s. represents the divergence of the heat flux due to e. g. conduction. Other sources of the heating or cooling, summarized above, are included in the term H. This energy-balance equation constrains the temperature profile of the prominence or its fine-structure parts. However, it is interesting to investigate the possibility that prominences or their fine structures are in radiative equilibrium, which means that no *extra* heating is needed.

The radiative-equilibrium models were first computed in detail by Heasley & Mihalas (1976). While the temperature at the surface of the 1D slab was 7 200 K, the central parts of their MHS models were too cool with temperatures even below 5 000 K. This was explained by inefficient penetration of the hydro-

gen Lyman-continuum ionizing radiation into the slab. On the other hand, the optically-thin Balmer continuum can ionize the central regions more easily. However, the central temperatures are not consistent with the radiation temperature of the diluted incident Balmer-continuum radiation as we show below. The issue of radiative equilibrium in prominence hydrogen threads was recently reinvestigated by Gouttebroze (2007). While the surface temperatures are consistent with those found in earlier works, the central ones are definitely higher, above 5 500 K.

The radiative equilibrium with enhanced central temperatures can be established by considering a more efficient penetration of the ionizing Lyman-continuum radiation into the slab (Heasley & Mihalas 1976), which represents a prototype of heterogeneous models. Heasley & Mihalas (1976) have also considered an arbitrary heating function H in some of their models. The conductive heating was generalized by Fontenla et al. (1996) who considered the ambipolar diffusion mechanism. However, their hydrogen Lyman-line intensities, in particular Lβ, are unrealistically high as recently shown by Vial et al. (2007) and Gunár et al. (2010).

In the following subsection we will briefly describe our new results which concern the radiative losses in cool parts.

2.2. Radiative equilibrium reconsidered

Vernazza et al. (1981) have already shown that dominant chromospheric coolants are hydrogen, singly ionized calcium and magnesium. In order to determine the importance of Ca II radiative losses for prominence plasmas, we have computed several 1D slab models using our recent versions of the non-LTE multilevel codes for hydrogen and calcium. The hydrogen code uses a 5-level plus continuum model atom with partial redistribution in the Lα and Lβ lines and the hydrogen radiative losses/gains were computed with this code in the same way as in Anzer & Heinzel (1999). The calcium code previously used by Anzer & Heinzel (1999) was later modified and extensively tested against the results of a similar code developed at IAS by P. Gouttebroze. As a result, new hydrogen and calcium modeling of prominences was presented by Gouttebroze & Heinzel (2002). An important feature of the modified Ca II code is the consistent treatment of the Ca II ionization by the UV radiation of hydrogen Lyman lines and continuum. We use this new version of the calcium code to compute the Ca II radiative losses. However, in contrast to Gouttebroze & Heinzel (2002), we apply here the complete redistribution approximation for the Ca II H and K resonance lines. The reason is that the complete redistribution leads to higher losses in the Ca II lines as compared to those computed with more realistic partial redistribution and this excess mimics, to a certain degree, the losses by the Mg II resonance lines h and k which we neglect here. Therefore, our results for Ca II losses in this paper are in fact showing the importance of both the Ca II and Mg II losses. The same approach was recently used by Carlsson (2009) for numerical simulations of the quiet solar chromosphere. The net radiative losses are defined by Eq. 7.

Our models are represented by 1D plasma slabs standing vertically above the solar surface and illuminated from both sides symmetrically by the incident solar radiation. They may represent both the whole prominence having a geometrical thickness of a few thousands km, as well as the fine-structure elements with much smaller thickness. In order to compare our results with those recently obtained for pure hydrogen by Gouttebroze (2007), we consider two sizes of the slab with the geometrical thickness D = 200 km and D = 5 000 km (the models of Gouttebroze (2007) represent vertical cylinders with the same values of diameters). We use three values of the gas pressure, $p = 0.01, 0.1$ and 0.5 dyn cm^{-2}, the same as in Gouttebroze (2007). All models use a constant microturbulent velocity of 5 km sec^{-1}. Helium is taken into account for the density determination but it does not contribute to the electron density. The helium abundance is 0.1, for calcium we take a value of 2.19×10^{-6}.

In this exploratory study we do not solve the full energy-balance problem as in Heasley & Mihalas (1976) or Gouttebroze

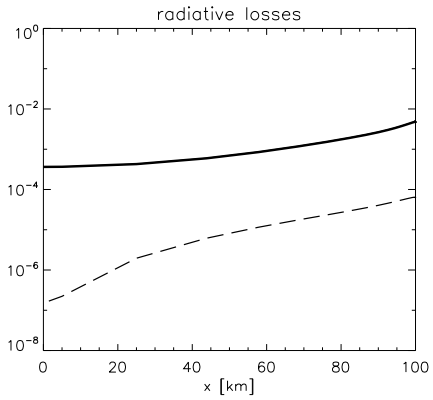

Fig. 3. Radiative losses (in erg s^{-1} cm^{-3}) for the model with $p = 0.1$ dyn cm^{-2}, $D = 200$ km and $T = 7\,100$ K. The full line shows the total hydrogen and calcium losses, while the dashed line corresponds only to the purely hydrogenic gains. Only one half of the symmetrical slab is displayed.

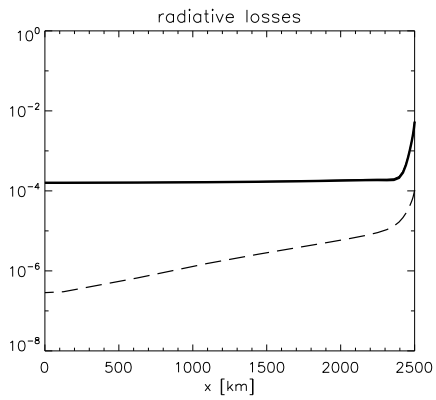

Fig. 4. Same as in Fig. 3, but for $D = 5\,000$ km and $T = 6\,800$ K.

(2007), but rather we try to find such isothermal-isobaric models which have zero radiative losses around the central parts. The kinetic temperature of the slabs found in this way gives us an idea about the radiative-equilibrium temperature in their central parts, although the true values may somewhat differ if the whole slab is enforced to be in radiative equilibrium.

For the set of six isothermal-isobaric models (two values of D and three values of p), we have determined the kinetic temperatures for which the net radiative losses in the central parts are zero or, more specifically, for which the losses turn into gains. These 'radiative-equilibrium' temperatures $T_{\rm re}$ are summarized in Table 1.

First we have considered only the hydrogen losses like in a recent study by Gouttebroze (2007). Using the same incident Lyman-continuum radiation, we arrived at temperatures qualitatively similar to those of Gouttebroze (2007). Actually ours are systematically higher which is consistent with the fact that Gouttebroze (2007) has used the complete redistribution for hydrogen lines. Other differences are presumably due to the different geometry (slabs vs. cylinders) and also due to our approximate approach to determine $T_{\rm re}$. At lower pressures, our temperatures are lower, while for higher pressures they somewhat exceed the values for true radiative equilibrium in cylinders. Note that the losses from cylinders should be generally larger than from equivalent slabs. But despite of these differences, our results fully confirm the important conclusion of Gouttebroze (2007) that pure hydrogen models which are in radiative equilibrium never have central temperatures as low as previously found by Heasley & Mihalas (1976).

The rather high temperatures obtained for the lowest pressures are the result of an increasing radiation temperature $T_{\rm r}$ of the incident Lyman-continuum radiation with decreasing wavelength. This can be easily demonstrated by considering just a constant $T_{\rm r}$ which we set to the value at 912 Å, i.e., $T_{\rm r} = 6\,500$ K. The results are shown in the second part of our Table 1, where the $T_{\rm re}$ at lowest pressure are much lower, between 6 500 and 7 000 K. In parentheses we indicate the Lyman-continuum head optical thickness. We see that at low pressures the optical thickness is small and going to lower wavelengths, it decreases as λ^3. This allows the incident radiation at higher $T_{\rm r}$ to heat up the central parts of the slab. At higher pressures, where the optical thickness significantly grows, the Lyman-continuum $T_{\rm r}$ plays no longer the role and the results are identical with those for true solar irradiation. But the

Table 1. Radiative-equilibrium temperatures at slab center (in K). $f(\lambda)$ is the observed wavelength-dependent radiation temperature of the incident Lyman-continuum radiation. For the second set of models, the numbers in parentheses indicate the optical thickness of the 1D slab at the head of the Lyman continuum.

p[dyn cm^{-2}]	0.01	0.1	0.5	model
D = 200 km	8 600	7 100	6 900	H I losses only, $T_r = f(\lambda)$
D = 5 000 km	7 900	6 800	6 500	
D = 200 km	6 500 (0.2)	7000 (6)	6 900 (46)	H I losses only, T_r = 6 500 K
D = 5 000 km	7 000 (4)	6 800 (168)	6 500 (1380)	
D = 5 000 km	6 800	7 000	6 500	H I losses only, T_r = 8 000 K
D = 200 km	8 600	5 200	4 900	H I + Ca II losses, $T_r = f(\lambda)$
D = 5 000 km	5 200	4 900	4 300	

fact that T_{re} saturates for the thickest models to 6 500 K seems to indicate a direct relation to T_r = 6 500 K of the incident Lyman-continuum radiation. However, a closer inspection shows that this is not the case.

To show this we have increased the incident T_r to 8 000 K and found the same central T_{re} = 6 500 K – see the third set of models in Table 1. We do not want to overinterpret our simple estimates of the central T_{re}, but it seems plausible that this equilibrium temperature saturates to values around 6 500 K, independently of the intensity of the photoionizing Lyman continuum and with a negligible dependence on the slab thickness D. Moreover, this value can hardly be explained by the role of the optically-thin Balmer continuum which has a much lower T_r = 5 500 K in our case (we use data from Table IV of Rudawy & Heinzel 1992). The role of the Balmer continuum was suggested by Heasley & Mihalas (1976) who arrived at much lower central equilibrium temperatures, well below 5 000 K. For the 1D cylinders of Gouttebroze (2007), the central T_{re} also saturates to 6 500 K for D = 200 km, while for large D = 5 000 km it saturates below 6 000 K.

Finally, we show in Table 1 our new results for a mixture of hydrogen and calcium. For small D = 200 km and for the lowest pressures, the central T_{re} is similar to that obtained for pure hydrogen models which indicates the negligible role of calcium losses. In other words, very small fine structures would need no additional heating provided that the gas pressure is of the order of 10^{-2} dyn cm^{-2} or lower. Such a situation seems to be rather unrealistic – see 2D fine-structure modeling of Gunár et al. (2010) based on SOHO/SUMER observations. However, for higher pressures and thicknesses, the Ca II losses start to be significant and they compensate for hydrogen gains at lower temperatures. As a result, much lower temperatures are obtained in comparison to a pure hydrogen plasma. For p = 0.5 dyn cm^{-2} and D = 5 000 K we arrived at T_{re} as low as 4 300 K, a value surprisingly similar to those of Heasley & Mihalas (1976) for hydrogen-helium slabs.

The radiative losses as the function of depth in 1D slabs are shown in Fig. 3 and Fig. 4, for two different models. The dashed lines correspond to negative hydrogen losses (gains) which turn into losses around the central parts when the temperature is increased. The full line shows the total losses due to hydrogen and Ca II and we see that they are more than two orders of magnitude larger as compared to pure hydrogen. Therefore, the central equilibrium temperatures are lowered as shown in Table 1. We have also found that the complete redistribution in Lα and Lβ lines leads to higher losses as compared to the partial-redistribution case used in producing the Table 1 and the two plots shown here. This behavior is consistent with that found for Ca II by Carlsson (2009).

The very low central temperatures obtained by Heasley & Mihalas (1976) have been explained by the authors as due to the equilib-

rium with the optically-thin Balmer continuum radiation which fully penetrates into the slab center and is determined by the photospheric intensity. However, our results point to a more complex scenario. Our Balmer continuum has $T_r = 5\,500$ K, which gives even lower irradiation when the dilution factor is taken into account. Therefore, the central temperatures around 6 500 K, found in all our thickest models, can hardly be explained by this photoionization equilibrium. We made several sensitivity tests and found that this particular central temperature is due to both the excitation rate by the Lα radiation field, giving the hydrogen second-level population, and the photoionization rate from that level due to the Balmer continuum. For example, by changing artificially the incident Lα radiation, the central equilibrium temperature also changes. And since the Lα line is formed under partial-redistribution conditions, the resulting temperature will also depend on this (note that Heasley & Mihalas 1976 used complete redistribution).

3. Conclusions

In this paper we have focused on two important aspects of the prominence physics: the fine-structure equilibria and prominence energetics. Multi-thread models with 2D or 3D radiative transfer and mutual radiative interaction certainly represent a vivid scenario. Future measurements of the magnetic field have to discriminate between vertically-aligned force-free dips (Dudík et al. 2008) and gravity-induced dips modeled here. Purely hydrogenic models of fine-structure threads (a few hundreds km thick) in radiative equilibrium would lead to realistic temperatures, however, adding the radiative losses by other elements (Ca II, Mg II) again results in too low central temperatures. A realistic energy-balance modeling within 2D or 3D filamentary structures, based on reasonable heating mechanisms, thus represents a great challenge.

Acknowledgements. PH and SG acknowledge the support from grants 205/09/1705 and 205/09/P554 of the Grant Agency of the Czech Republic. This work was also supported by ESA-PECS project 98030 and the institutional project AV0Z10030501.

References

Anzer, U., & Heinzel, P. 1999, A&A, 349, 974
Anzer, U., & Heinzel, P. 2008, A&A, 480, 537
Auer, L.H., & Paletou, F. 1994, A&A, 285, 675
Berger, T. E., Shine, R.A., Slater, G. L., et al. 2008, ApJ, 676, L89
Carlsson, M. 2009, private communication
Dudik, J., Aulanier, G., Schmieder, B., Bommier, V., & Roudier, T. 2008, Sol. Phys., 248, 29
Fontenla, J., Rovira, M., Vial, J.-C., & Gouttebroze, P. 1996, ApJ, 466, 496
Gouttebroze, P. 2007, A&A, 465, 1041
Gouttebroze, P., & Heinzel, P. 2002, A&A, 385, 273
Gunár, S., Schwartz, P., Schmieder, B., Heinzel, P., & Anzer, U. 2010, A&A, in press
Heasley, J. N., & Mihalas, D. 1976, A&A, 205, 273
Heinzel, P. 1995, A&A, 299, 563
Heinzel, P., & Anzer, U. 2001, A&A, 375, 1082
Heinzel, P., & Anzer, U. 2010, A&A, submitted
Heinzel, P., Schmieder, B., Fárník, F., et al. 2008, ApJ, 686, 1383
Kippenhahn, R., & Schlüter, A. 1957, ZAp, 43, 36
Paletou, F. 1995, A&A, 302, 587
Parenti, S., & Vial, J.-C. 2007, A&A, 469, 1109
Rudawy, P., & Heinzel, P. 1992, Sol. Phys., 138, 123
Rybicki, G. B., & Hummer, D.G. 1991, A&A, 245, 171
Schmieder, B., Chandra, R., Berlicki, A., Mein, P., Molodij, G., & Berger, T. 2010, A&A, in press
Vernazza, J. E., Avrett, E. H., & Loeser, R. 1981, ApJS, 45, 635
Vial, J.-C., Ebadi, H., & Ajabshirizadeh, A. 2007, Sol. Phys., 246, 327